Investigation of Effects of Processing on Stretch-Flangeability of the Ultra-High Strength, Vanadium-Bearing Dual-Phase Steels

Yingjie Wu[1], Juha Uusitalo[2] and Anthony J. DeArdo[1,2]*

[1] Basic Metals Processing Research Institute, Department of Mechanical Engineering and Materials Science, Swanson School of Engineering, University of Pittsburgh, 636 Benedum Hall, 3700 O'Hara Street, Pittsburgh, PA 15261, USA.

[2] Centre for Advanced Steels Research, Materials Engineering Laboratory, Department of Mechanical Engineering, University of Oulu, P.O Box 4200, FI-90014, Oulu, Finland.

ORCID numbers of all authors and the email address of the corresponding author:

Y. Wu: 0000-0002-7062-7568

J. Uusitalo: 0000-0001-7393-6465

A. J. DeArdo*: 0000-0003-3485-4496; deardo@pitt.edu (Corresponding co-author).

Abstract

The purpose of this paper was to gain a better insight into the sheared-edge ductility of high strength dual-phase steels for the purpose of helping improve the hole expansion behavior of such steels. A candidate dual-phase (DP) steel in this study was designed and processed with distinct coiling temperatures after conventional finish rolling, and then further processed with two continuous galvanizing line (CGL) simulations. Two CGL simulations with slightly different thermal paths were conducted on a Gleeble 3800 machine; one was to replicate standard galvanizing (GI), where the intercritically annealed steels were cooled to the zinc pot temperature, and the other one was a supercooling process (SC) where the intercritically annealed steels were first cooled to the M90 temperature of the intercritically formed austenite, then up-quenched to the zinc pot temperature. The findings indicated that the combination of a low coiling temperature and GI anneal can obtain the microstructures characterized by a high-volume-percentage of martensite and fine-grained ferrite with a high tensile strength (UTS) of 1092.8 MPa and a good total elongation (TE) of 20.8%. A large amount of fresh martensite was replaced by tempered martensite caused by the changes in CGL thermal paths from GI to SC anneals, resulting in the considerable

increase in sheared-edge ductility properties, although with a loss of UTS. Additionally, the damages caused by hole punching were examined by electron backscattered diffraction (EBSD) - kernel average misorientation (KAM) and nanoindentation technologies. These results showed that the micro-voids or micro-cracks in the initial punched hole surfaces and plastic internal strains near the initial punched hole sheared edges introduced by hole punching will severely influence stretch-flangeability.

Keywords: Dual-Phase (DP) Steels, Hole Expansion Ratio, Coiling Temperatures, Continuous Galvanizing Line (CGL), Hole Punching, Electron Backscattered Diffraction (EBSD), Kernel Average Misorientation (KAM), Nanoindentation.

1. Introduction

Since the advanced high strength steels (AHSS) simultaneously increase strength, reduce mass, improve safety and lower CO_2 emissions, they have continued to be attractive to the automotive industry. Perhaps the most popular of the AHSS are the dual-phase (DP) steels. The final microstructures of dual phase steels consist of ductile ferrite and the controlled amounts of fresh martensite or with other phases, such as bainite, tempered martensite or retained austenite [1–8] in order to achieve the strength-formability-crash worthiness required. DP steels are considered as good combination of high strength and reasonable ductility (both total elongation (TE) and shear-edge ductility). In terms of ductility, studies of DP steels from the mid-1970s showed many factors were governing the TE, including grain sizes, ferrite volume fraction and inclusions. Furthermore, recent literature [17–21] reported that increasing the amount of retained austenite may improve TE due to transformation induced plasticity (TRIP) or TRIP effect. Therefore, TRIP steels [22], and later quench and partitioning (Q&P) steels [23] were developed.

Sheared-edge ductility is another aspect of ductility. Hole expansion ratio (HER) is an important parameter used to evaluate the sheared-edge ductility of metal sheets [24]. HER can be determined by performing a hole expansion test (HET), where a steel sheet (100 mm × 100 mm) with a punched hole (10 mm in diameter) in the center is pierced by a conical punch to expand the hole. The test is not terminated until a through-thickness crack occurs. Hence, HER values can be obtained by applying Equation 1 [24–27].

$$HER = \frac{D_h - D_o}{D_o} \times 100\% \quad (1)$$

where, D_o and D_h are the original and final inner hole diameters, respectively.

From previous literature [28–30], the microstructures, especially the hard constituents, such as martensite, bainite or cementite, of DP steels can affect HER values. Terrazas et al. [30] found that hole expansion performance was improved as the number of the martensite constituents per unit area increased. Also, the product of martensite size, contiguity and martensite mean free distance had a positive linear relation with HER [30]. Moreover, the hardness difference between the soft phase (ferrite) and the hard constituents is considered a critical factor controlling HER. Decreasing the hardness difference between soft phase and hard constituents helps to improve the hole expansion property [13,31,32]. Thus, the HER values will be improved, as ferrite is strengthened with second-phase precipitates or hard fresh martensite is replaced with relatively softer phases or microconstituents, such as pearlite [25], bainite or tempered martensite [33].

Furthermore, the approaches used in the initial hole formation before HET also influence HER values. In most cases, the holes of HER specimens are formed by cold punching, since it is the fastest and most economical way of forming a hole. In the research of Yoon et al. [24], the hole expansion performances of the samples with the initial punched holes were worse than those of the specimens with the milled holes, since the subsequent milling process can remove the most part of the shearing damages and the micro-cracks caused by the punching process [31,34–38]. Moreover, Taylor et al. [13] found that the HER blanks with the EDM holes had higher HER values, compared with the those with the punched holes, since the shear affected zone (SAZ) was absent concerning the EDM holes.

In the present research, in order to obtain high hole expansion performances of ultra-high strength DP steels, the candidate steels were explored with different pre-annealing condition, i.e., coiling temperature, and continuous galvanizing line (CGL) simulations, one a conventional standard galvanizing and the other one was supercooled to the temperature (near the M90 temperature) after anneal and immediately up-quenched to zinc pot temperature. The microstructures, uniaxial tensile properties and stretch-flangeability of these DP steel conditions were identified and compared. Additionally, in order to investigate the crack initiation caused by hole punching, the microstructural damages after punching were observed via SEM. And the

internal plastic strains near the initial hole punched hole sheared edges were determined by EBSD-KAM and nanoindentation technologies.

2. Experimental Procedure

2.1. Chemistry and processing

A candidate DP steel (chemistry in wt. %: 0.15 C, 2.0 Mn, 0.01 P, 0.003 S, 0.4 Si, 0.02 Cu, 0.01 Ni, 0.5 Cr, 0.005 Mo, 0.004 Ti, 0.06 V, 0.005 N and 0.06 V) was prepared by vacuum induction melting and solidifying in cast iron ingot molds. For rough rolling, the ingots were reheated to 1250°C, followed by rough rolling to 25 mm in several passes. In terms of finishing rolling, the steels were reheated again to 1250°C and hot rolled in 5 passes, with each reduction of about 27.5%, to the final thickness of 5 mm, with the finishing rolling temperature (FRT) of approximately 920°C. Subsequently, the steels were water spray cooled to the coiling temperature of 677°C (the steel condition was labeled by A1) or 580°C (labeled by A2) at a cooling rate of approximately -30°C s^{-1}, followed by controlled cooling to the room temperature (RT) at approximately -30°C h^{-1}. In addition to the surface grinding, during which the oxide layers and impurities on the surface of hot band coils were removed and the desired surfaces were obtained with the thickness of 3 mm. After being 60% cold rolled to the final thickness of 1.2 mm, the cold rolled steels were sectioned for the CGL simulations conducted on a Gleeble 3800 machine. There were two CGL simulations employed: one was a standard galvanizing (labeled by GI) and the other one was a supercooling process (labeled by SC). The major thermomechanical processing and heat treatments consisting of hot rolling, coiling, surface grinding, cold rolling and CGL simulations are presented in Figure 1. For the GI anneal simulation, the cold rolled steel conditions were reheated for annealing at +5°C s^{-1} to 780°C (seen in Figure 1). After the 60-second isothermal holding, the samples were controlled cooled to the zinc pot temperature (~ 460°C) at a cooling rate of -15°C s^{-1} and soaked for 15 s in an effort to simulate hot dipping and to retard the formation of ferrite and bainite. Finally, the samples were fast cooled to room temperate at a cooling rate of -10°C s^{-1} to obtain a large amount of fresh martensite. Regarding the SC anneal, the reheating section was similar to that of GI anneal, while after the 60-second isothermal anneal holding, the samples were fast cooled to the supercooling temperature of 250°C (near the M90 temperature) at -15°C s^{-1} and held 20 s. Then, the samples were up quenched to 460°C at +42°C s^{-1} and held 15 s

to obtain a large percent of tempered martensite, followed by fast cooling to RT at a cooling rate of -10°C s^{-1}.

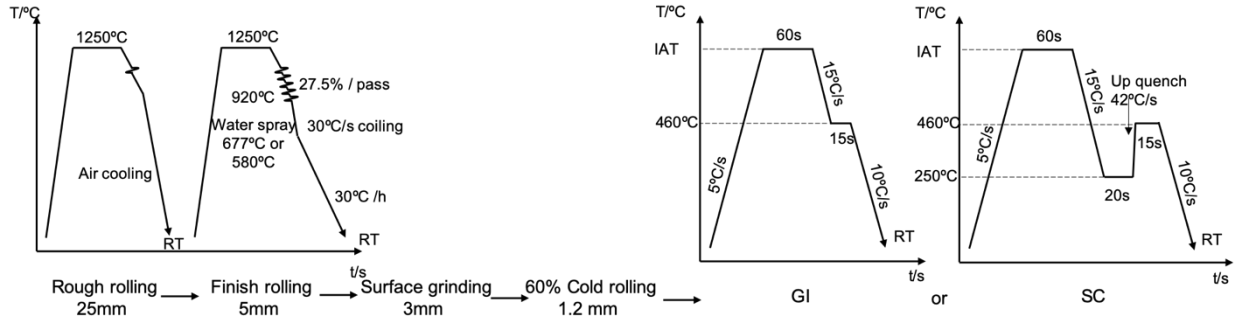

Figure 1 The schematic process containing hot rolling, surface grinding, cold rolling and CGL simulations

2.2. Mechanical testing

Tensile tests were completed by a ZwickRoell Z100 tensile testing machine, according to ASTM E8. The steels with different conditions were machined into sub-sized tensile samples with a gage length of 10 mm along the transverse direction (TD). The basic uniaxial tensile properties were recorded and will be discussed in the following sections.

2.3. Hole expansion testing

The hole expansion tester of BAMPRI was reconstructed from a vintage Tinius Olsen formability tester [43] and the conical punch and dies were designed and manufactured to meet the requirements of ISO/TS 16630 standard. Once the test was in place, its validity was verified by a round robin test, involving the punched specimens of high strength dual-phase (HSDP) steels supplied by United States Steel (USS) corporation. The strain rate applied by a conical punch was continuous and constant (~ 0.3 cm s^{-1}). However, since the CGL annealing simulations of the BAMPRI developed steels were to be conducted on a Gleeble 3800 machine, it was not possible to test the usual 100 mm × 100 mm square specimens containing a 10 mm punched hole in the center. The largest Gleeble annealed blanks that could be annealed were 100 mm in length × 80 mm in width and contained a uniform heated zone of about 30 mm in diameter at the center. These 100 mm × 100 mm specimens were tested against the 100 mm × 80 mm specimens with good reproducibility.

2.4. Material characterizations

In terms of material characterizations, the samples were sectioned, and the surface of each steel condition was ground with 600~1200 grit SiC abrasive grinding papers. After mechanical grinding, the samples were polished by a Buehler VibroMet^{TM} 2 vibration polisher for 45 - 60 min with 0.05 μm alumina suspension. Then, each sample was etched by a 2% Nital reagent for the observation of OM and the FEI Apreo SEM.

2.5. Measurements of plastic strains caused by hole punching

In order to investigate the local internal plastic strains caused by punching for fully CGL - annealed DP steels. The initial punched hole sheared edges of several conditions were selected and tested via EBSD and nanoindentation technologies. Figure 2 schematically shows the initial punched hole sheared edge with four thoroughly tested positions. Position (A) is the region in the sheared edge near the burnished and fracture transition zone; position (B) is in the sheared edge near the middle of the fracture zone; position (C) is in the shear affected zone (SAZ) and 300 μm away from position (B); and position (D) is in the sheared edge near the bottom of the fracture zone.

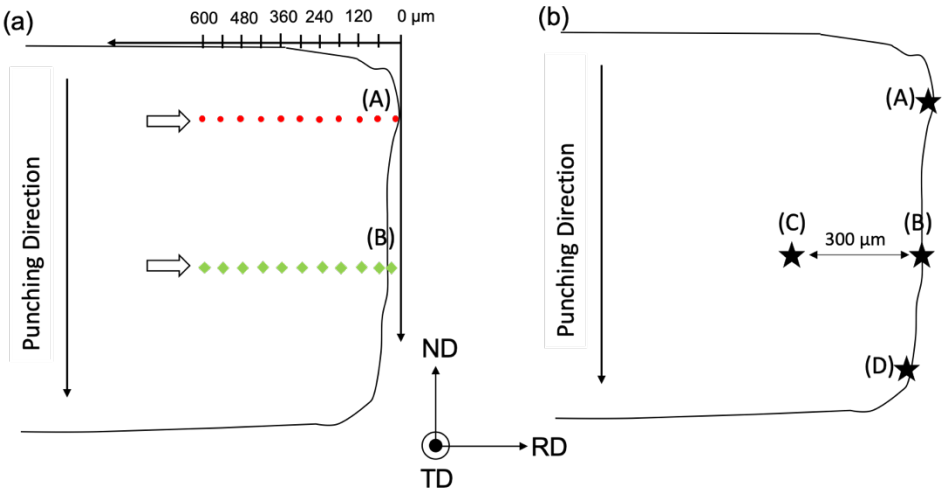

Figure 2 The schematic illustrations of the initial punched hole sheared edges of selected fully annealed DP samples with the tested positions for (**a**) EBSD-KAM and (**b**) nanoindentation technologies.

For EBSD-KAM method, the pre-strain conditions of the areas with the distances of 0 μm to 600 μm away from the position (A) (near the burnished and fracture transition zone) or position (B) (near the middle of the fracture zone) were examined by a FEI Scios Dual Beam SEM attached with a EBSD detector, with an accelerating voltage of 20 kV, a current of 13 nA or a spot size of

15, a working distance of 14 mm, a SEM magnification of 2000 ×, a step size of 0.1 μm and a mapping area of 30 μm × 30 μm. An OIM Analysis™ software was utilized to analyze and provide detailed information on crystallographic orientations, deformed grain shapes and local deformation caused by punching in this research. Nakada et al [46] combined EBSD-KAM and digital image correlation (DIC) technologies to establish a critical correlation between KAM values and local equivalent strains (ε_{eq}) caused by plastic deformation for DP steels. This correlation is shown in Equation 2 [46], illustrating that KAM values obtained by the EBSD method can be expressed as a function of equivalent strains measured by the DIC approach .

$$\text{KAM (rad)} = \frac{\pi}{180} \times 1.68\ \varepsilon_{eq}^{0.44} \tag{2}$$

So, the specific local internal plastic strains caused by hole punching can be directly calculated with the application of Equation 3, converted from Equation 2, based on EBSD-KAM values (in degree).

$$\varepsilon_{eq} = \sqrt[0.44]{\frac{\text{KAM (°)}}{1.68}} \tag{3}$$

In terms of nanohardness approach, the nanohardness results of the deformed microstructures, like soft ferrite and hard constituents, in positions (A) to (D) were tested and calculated, shown in Figure 2 (b). A 5 × 5 square pattern of indentations was performed on the final polished surface for each position with a load of 2000 μN, using a HYSITRON TI 900 TriboIndenter® with a Berkovich indenter tip. Times of loading and unloading for every single indentation were 10 s each. The distance between each indentation was 6 μm to avoid the potential effect of overlapping plastic zones. After testing, the nanohardness of each nano-indent was calculated, by applying the Oliver-Pharr method, from the loading-displacement curve corresponding to each indentation [13].

3. Results

3.1 Microstructures after full CGL simulations

The typical final microstructures of simulated fully annealed DP steels with GI and SC anneals, produced on a Gleeble 3800 machine, are presented in Figures 3 and 4, respectively. Figure 3 shows the SEM micrographs of the GI annealed sample A1, GI (CT580℃, standard

galvanizing), consisting of ferrite, bainite and fresh martensite. The ferrite in the final microstructures of GI annealed DP steels includes old ferrite (recrystallized from the 60% cold rolled ferrite in the initial hot band during reheating from RT to the optimum IATs at a low heating rate of +5°C s^{-1}), and new ferrite (transformed from intercritically formed austenite during cooling from IATs at a cooling rate of -15°C s^{-1}) [47]. The formation of bainite occurs during a short-time holding (~15 s) at the a zinc pot temperature of 460°C (near or below the B_s temperature) [47]. Fresh martensite transforms from intercritically formed austenite by quenching at a fast cooling rate of -10°C s^{-1} from 460°C to RT. The SEM micrographs of the SC annealed sample for condition A1, SC (CT580°C, supercooling process) are shown in Figure 4. In addition to ferrite, bainite and fresh martensite mentioned above, the final microstructure of a SC annealed sample also includes tempered martensite, which formed during the up-quench to 460°C from the fresh martensite formed by quenching from IATs to the supercooling temperature of 250°C. A large amount of fresh martensite is replaced with tempered martensite by up-quenching at a rate of +42°C s^{-1} from the supercooling temperature to the zinc pot temperature, resulting in the increases in both TE and HER, but with the loss of UTS. After the CGL simulations, the microstructural characteristics of four steel conditions (two coiling temperatures and two CGL simulations) were investigated in this study and are listed in Table 1.

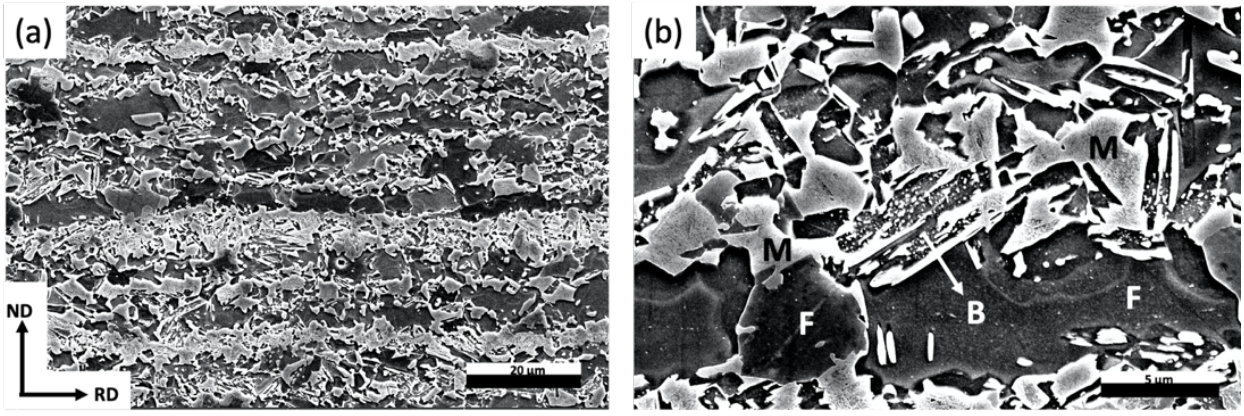

Figure 3 The SEM micrographs of the fully annealed sample for condition A1, GI (CT 580°C, standard galvanizing) with (**a**) low magnification and (**b**) high magnification. Note: Ferrite is labeled by F, bainite by B and fresh martensite by M.

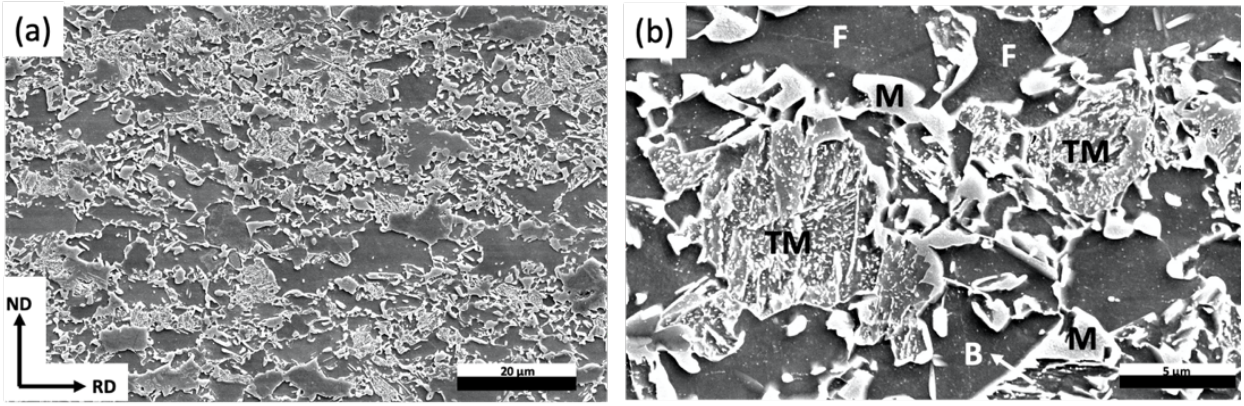

Figure 4 The SEM micrographs of the fully annealed sample for condition A1, SC (CT 580℃, supercooling process) with (**a**) low magnification and (**b**) high magnification. Note: Ferrite is labeled by F, bainite by B, fresh martensite by M and tempered martensite by TM.

Regarding the effect of two coiling temperatures on microstructural characteristics, first, decreasing coiling temperature from 677 ℃ to 580 ℃ can refine ferrite grains. For example, the average ferrite grain sizes of A1, GI (CT580℃, standard galvanizing) and A2, GI (CT677℃, standard galvanizing) are 3.9 μm and 5.1 μm, respectively (Table 1). Second, different coiling temperatures affect phase balance. The volume fractions of bainite and fresh martensite of A1, GI (CT580℃, standard galvanizing) are 29.5% and 48.8%, respectively (Table 1). For fully annealed sample A2, GI (CT677℃, standard galvanizing), the counterparts are 29.0% and 42.8% (Table 1). It should be noted that the total volume percentage of hard phase (bainite + fresh martensite) for A1, GI with a low coiling temperature is higher than that for A1, GI with a high coiling temperature. In terms of two annealing paths (GI and SC anneals), their effects on the final microstructures of fully annealed DP steels are apparent. The microstructures of DP steels with GI anneals include ferrite, bainite and fresh martensite (Figure 3). However, a considerable amount of fresh martensite is replaced with the relatively soft tempered martensite observed in the final microstructures of SC annealed DP steels (Figure 4). The microstructural features of steel conditions A1, GI and A1, SC illustrate this point clearly. The only difference between these two samples is the annealing path. The volume fraction of fresh martensite of A1, GI is 48.8% with the absence of tempered martensite, while the volume percentages of fresh martensite and tempered martensite of A1, SC are 25.6% and 30.1%, respectively. The replacement of fresh martensite with tempered martensite leads to the large differences in the mechanical properties (i.e., UTS, TE and HER) between GI and SC annealed DP steels, observed in Tables 2 and which were discussed in the following section.

Table 1

The microstructural features (average ferrite grain size (d_α), volume percentages of ferrite ($fv_{(F)}$), bainite ($fv_{(B)}$), fresh martensite ($fv_{(M)}$) and tempered martensite ($fv_{(TM)}$) of fully annealed samples with different conditions.

IDs	Conditions	d_α (μm)	$fv_{(F)}$ (%)	$fv_{(B)}$ (%)	$fv_{(M)}$ (%)	$fv_{(TM)}$ (%)
A1, GI	CT580℃, standard galvanizing	3.9 ± 1.0	21.7	29.5	48.8	0
A2, GI	CT677℃, standard galvanizing	5.1 ± 1.9	28.2	29.0	42.8	0
A1, SC	CT580℃, supercooling process	4.2 ± 1.4	33.2	11.1	25.6	30.1
A2, SC	CT677℃, supercooling process	5.7 ± 1.9	30.3	7.5	19.0	43.2

3.2. Mechanical properties

The mechanical properties including hole expansion ratio (HER), ultimate tensile strength (UTS) and total elongation (TE) of the fully annealed DP steels with different conditions are listed in Table 2.

Table 2

Mechanical properties (HER, UTS, and TE) of the fully annealed DP steels with different conditions.

IDs	HER (%)	UTS (MPa)	TE (%)
A1, GI	17.0	1092.8	20.8
A2, GI	14.6	1039.1	17.9
A1, SC	27.5	974.7	22.2
A2, SC	24.3	936.5	19.6

From Table 2, the highest UTS value was 1092.8 MPa for steel condition A1, GI (CT580℃, standard galvanizing). While, the best ductilities were 22.2 % (global ductility, TE) and 27.5 % (local ductility, HER) for steel condition A1, SC (CT580℃, supercooling process). Both UTS and ductility (TE and stretch-flangeability) are affected by coiling temperature and annealing path. Tensile strength increases as coiling temperature falls. For example, the UTS of A1, GI (CT580℃) is higher than that of A1, GI (CT677℃). Meanwhile, decreasing coiling temperature also results

in higher TE and HER results. Additionally, concerning the effect of annealing path on properties, the change in annealing path, from GI to SC anneals, gives a rise to TE and HER with a sacrifice of UTS.

3.3 Microstructural damages caused by punching

During hole punching but prior to hole expanding, the microstructures in the initial punched hole surface and sheared edge are deformed. Figures 5 shows the SEM micrograph of the initial punched hole surface of fully annealed steel condition A1, SC (CT580℃, supercooling process). The initial punched hole surfaces consist of zones of rollover, burnishing, fracture and shear burrs (Figures 5 (b)). A few micro-voids are observed in the burnished zone (Figures 5 (c)), and numerous micro-voids and shearing dimples exist in the fracture zone (Figures 5 (d) (e)), which is in accord with the observations of Yoon [34].

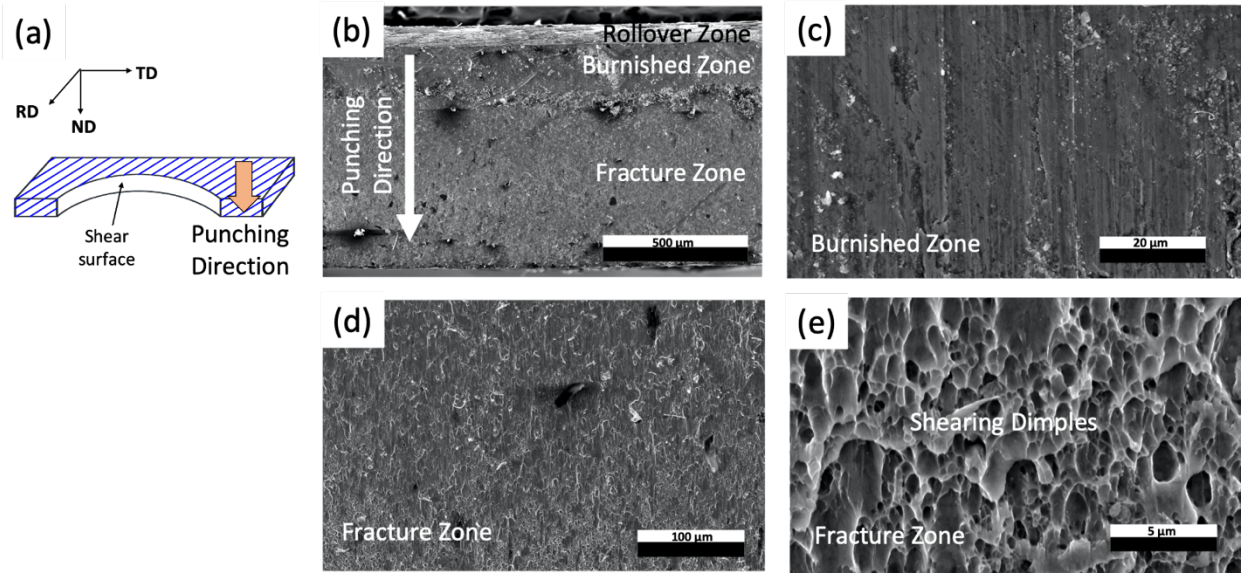

Figure 5 The SEM micrographs of the initial punched hole surface for sample LLL (0.04Al-0.06V-CT580℃-60%CR) SC after hole punching. (**a**) The schematic illustration; (**b**) the initial punched hole surface consisting of rollover, burnished and fracture zones; (**c**) the burnished zone with high magnification; (**d**) the fracture zone with low magnification and (**e**) shearing dimples in the fracture zone with high magnification.

Figures 6 shows the SEM micrograph of initial punched hole sheared edge with rollover, burnished, fracture zones and shear burrs indicated for steel condition A1, (CT580℃, supercooling process). Both the softer phase ferrite and harder components (i.e., bainite, fresh martensite or

tempered martensite) are deformed and elongated during plastic deformation caused by the hole punching process (Figures 6 (b),(d)-(f),(h)). Also, micro-voids and even micro-cracks can be observed in the sheared edge along the whole thickness direction near the rollover zone (Figure 6 (b)), burnished and fracture transition zone (Figures 6 (d)), fracture zone (Figures 6 (e), (f)) and shear burr (Figure 6 (h)). Also, it should be noted that the micro-voids in the sheared edge near the rollover zones exist at the ferrite/ferrite grain boundaries (Figure 6 (b)). The EDX analyses (Figures 6 (c) and (g)) illustrate the chemical compositions of the cracks observed in Figures 6 (b) and (f). The results indicate that those micro-cracks should be the inclusions of MnS or MnS & ZrO_3.

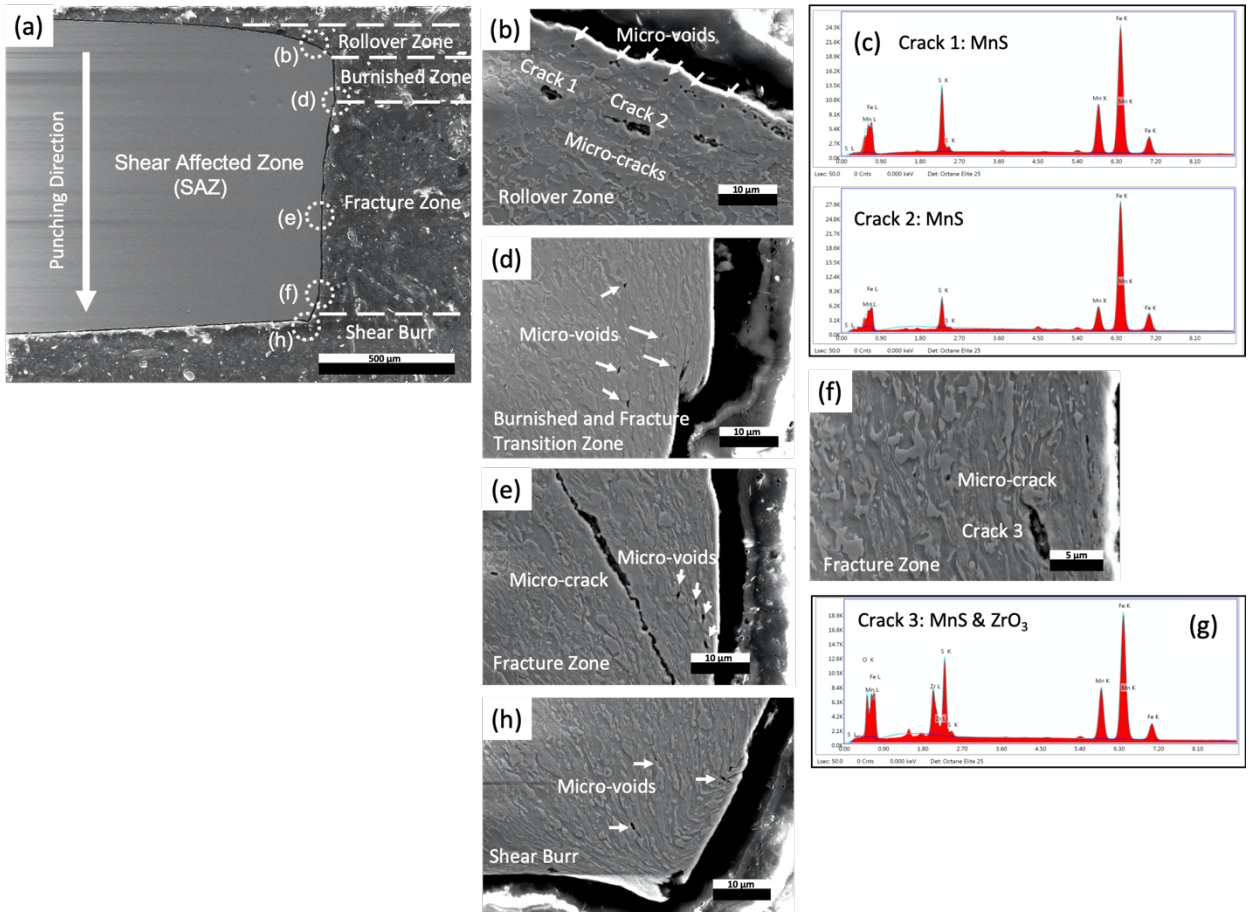

Figure 6 The SEM micrographs of the initial punched hole sheared edge for sample LLL (0.04Al-0.06V-CT580℃-60%CR) SC after hole punching. (**a**) The sheared affected zone (SAZ); (**b**) the micro-cracks near the rollover zones; (**c**) the EDX analyses of the cracks 1 & 2 in (**b**), presenting that both of them should be MnS; (**d**) the micro-voids near the burnished and facture transition zone; (**e**) the micro-crack and micro-voids near the middle of the fracture zone; (**f**) the micro-crack near the bottom of the facture zone; (**g**) the

EDX analysis of the crack 3 in (**f**) and the result shows that it is supposed to be MnS & ZrO_3; and (**h**) the micro-voids in the shear burr.

3.4. Local internal plastic strains introduced by punching

In order to investigate the local internal plastic strains introduced by punching for fully annealed DP steels with GI and SC anneals, the initial punched hole sheared edges of samples A1, GI (CT580℃, standard galvanizing) and A1, SC (CT580℃, supercooling process) were selected and examined via EBSD and nanoindentation technologies.

Figure 7 presents the inverse pole figures (IPFs) of oriented grains and microstructural-damage evolutions in the tested regions from the position A (in the initial punched hole sheared edge near the burnished and fracture transition zone) with the distances ranging from 0 μm to 600 μm for the sample A1, GI. Both ferrite and martensite grains were heavily deformed and elongated along the shear flow curves with high grain shape aspect ratios at position A due to hole punching (Figure 7 (b)). The impact of hole punching on the direction of elongation for those oriented grains gradually diminishes, as the distance from position A increases (Figures 7 (c)-(h)). When the distance exceeds 420 μm, both ferrite and martensite grains were barely elongated and influenced by hole punching, also possessing the similar grain shape aspect ratios as the ones of undeformed grains. (Figures 7 (i)-(l)).

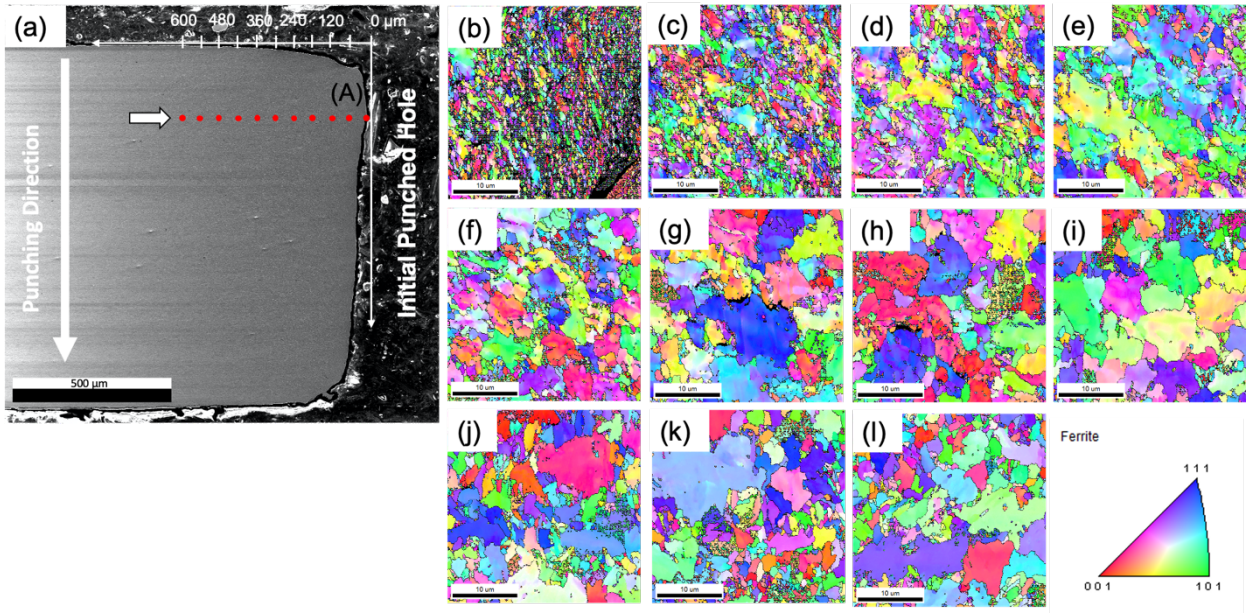

Figure 7 (a) The SEM micrograph schematically illustrating the tested positions, via EBSD technology, in the initial punched hole sheared edge for sample condition A1, GI (CT580°C, standard galvanizing) and the IPFs presenting the oriented grains in the tested regions away from position A (near the burnished and fracture transition zone) with the distances of (**b**) 0 µm, (**c**) 60 µm, (**d**) 120 µm, (**e**) 180 µm, (**f**) 240 µm, (**g**) 300 µm, (**h**) 360 µm, (**i**) 420 µm, (**j**) 480 µm, (**k**) 540 µm, and (**l**) 600 µm.

After hole punching, some dislocation structures are formed within the ferrite grains in the initial hole punched sheared edge or shear affected zone (SAZ), and the internal plastic strains are manifested as local variations in lattice orientation [44] which are also called lattice distortions. The measurement of the local misorientations within crystalline lattices (i.e., KAM methods) can reflect the amount of plastic deformation caused by hole punching. Also, the ε_{eq} can be calculated, by using Equation 3, from KAM values. The relations between the KAM values or equivalent strains (ε_{eq}) and the distance from the initial punched hole, in terms of position A and position B, of fully annealed DP steels with GI and SC anneals are plotted in Figure 8. Figure 8 shows that, both KAM values and ε_{eq} results decrease with increasing the distance from the initial punched hole. The convergences of KAM values and ε_{eq} results occur as the distance exceeds 400 µm, indicating that the sheared affected zones (SAZ) for both A1, GI and A1, SC conditions are about or less than 400 µm. In addition, there are large differences in KAM and ε_{eq} of the tested positions from position A and position B for both GI and SC annealed DP steels, at a distance less than 150 µm. As this distance is less than 150 µm, the KAM and ε_{eq} of the tested positions starting from

position A (near the burnished and fracture zone) are larger than those of the tested positions starting from position B (near the middle of the fracture zone), showing that the maximum strain occurred at the burnished and fracture transition zone [51]. Regarding the maximum strains at the burnished and fracture zones of both GI and SC annealed DP steels, the GI annealed DP sample A1, GI has a higher equivalent strain of 2.92 than the SC annealed DP sample A1, SC, of which the maximum equivalent strain is about 1.48. This indicates that the step of hole punching introduces more internal plastic strains along the initial punched hole sheared edge for the fully annealed DP steels with GI anneal and the damage caused by hole punching can severely influence the final HER values of GI annealed DP steels.

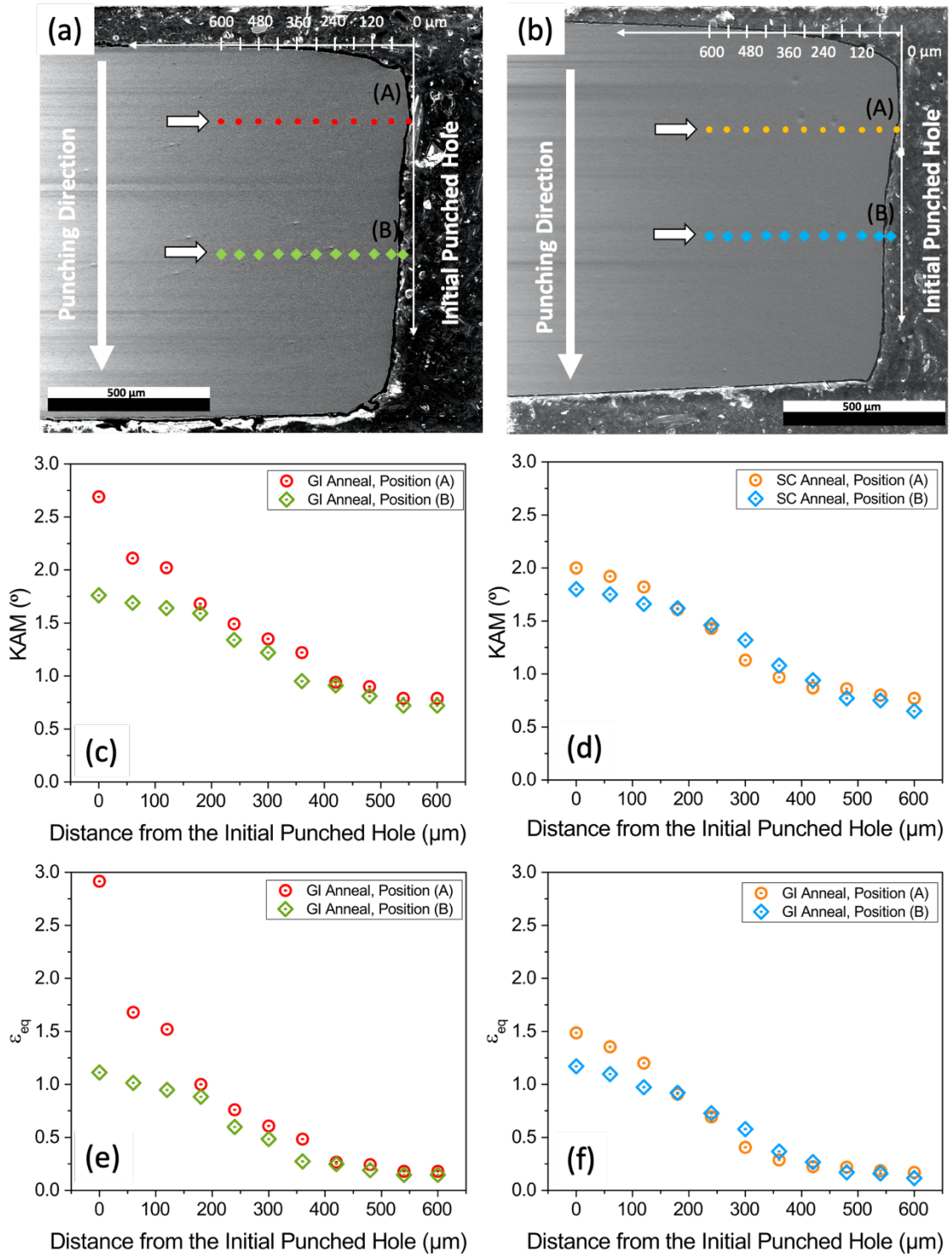

Figure 8 (**a**) The SEM micrographs schematically illustrating the tested positions with EBSD-KAM technologies as well as the relations between (**c**) KAM values or (**e**) calculated ε_{eq} results and the distance from the initial punched hole for the GI annealed DP sample A1, GI (CT580℃, standard galvanizing). (**b**) The SEM micrographs schematically illustrating the tested positions with EBSD-KAM technologies as well

as the relations between (**d**) KAM values or (**f**) calculated ε_{eq} results and the distance from the initial punched hole for the SC annealed DP sample A1, SC (CT580°C, supercooling process).

The SEM micrographs as well as the nano-indents of the tested positions in the initial punched hole sheared edges of fully annealed DP steels with both GI and SC anneals are shown in Figures 9 and 10, respectively. The ferrite and hard constituents (fresh martensite, bainite or tempered martensite) at the positions A, B and D in the initial punched hole sheared edge are heavily deformed and elongated along the shear flow curves (Figures 9 (b),(c),(e) and 10 (b),(c),(e)). Both ferrite and hard constituents are packed so tightly, with high grain shape aspect ratios, that the grain boundaries are difficult to observe. However, the microstructures in the position C, 300 μm away from the position B, are not severely influenced by hole punching (Figures 9 (d) and 10 (d)). Twenty-five nanoindentations of each tested position were observed via SEM. The nano-indents within the center of ferrite grains were marked by red circles, the ones within the center of fresh martensite grains by blue circles (for GI anneals), the ones within the center of tempered martensite grains by green circles (for SC anneals) and the ones in the regions containing ferrite/ferrite grain boundaries or ferrite/hard phase constituent interfaces by white circles.

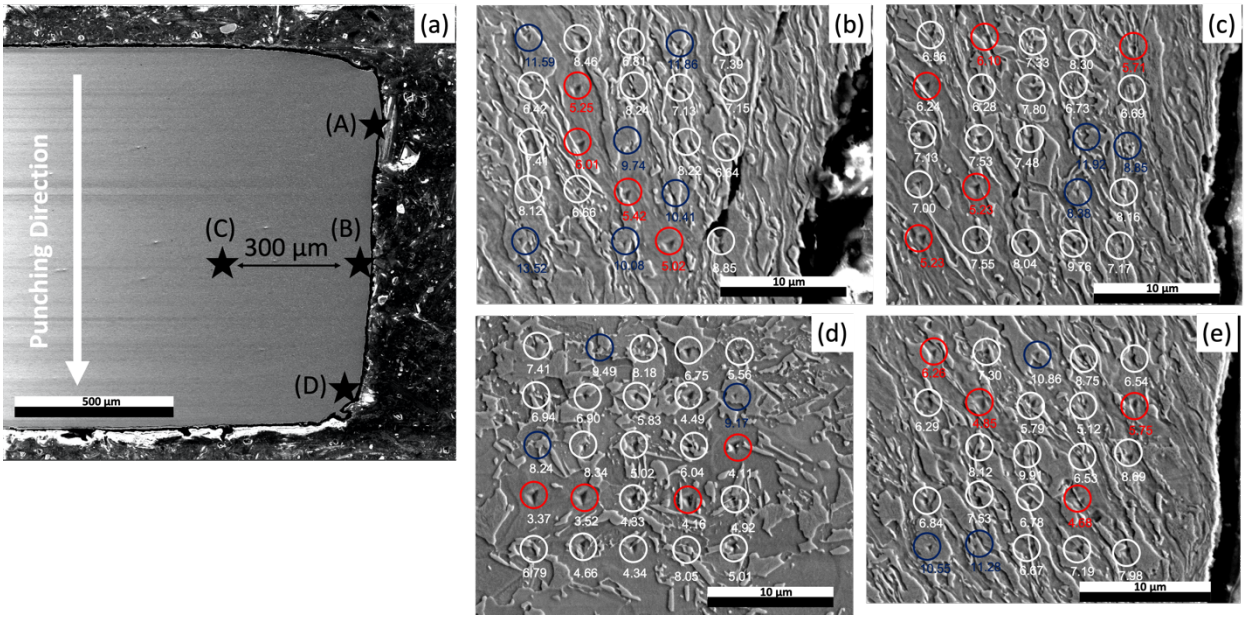

Figure 9 Nanoindentation tests for the initial punched hole sheared edge of the fully annealed DP steels with GI anneals. (**a**) The SEM micrograph schematically illustrating the tested positions. The SEM

micrographs as well as nano-indents of (**b**) position A, (**c**) position B, (**d**) position C and (**e**) position D with the high magnification.

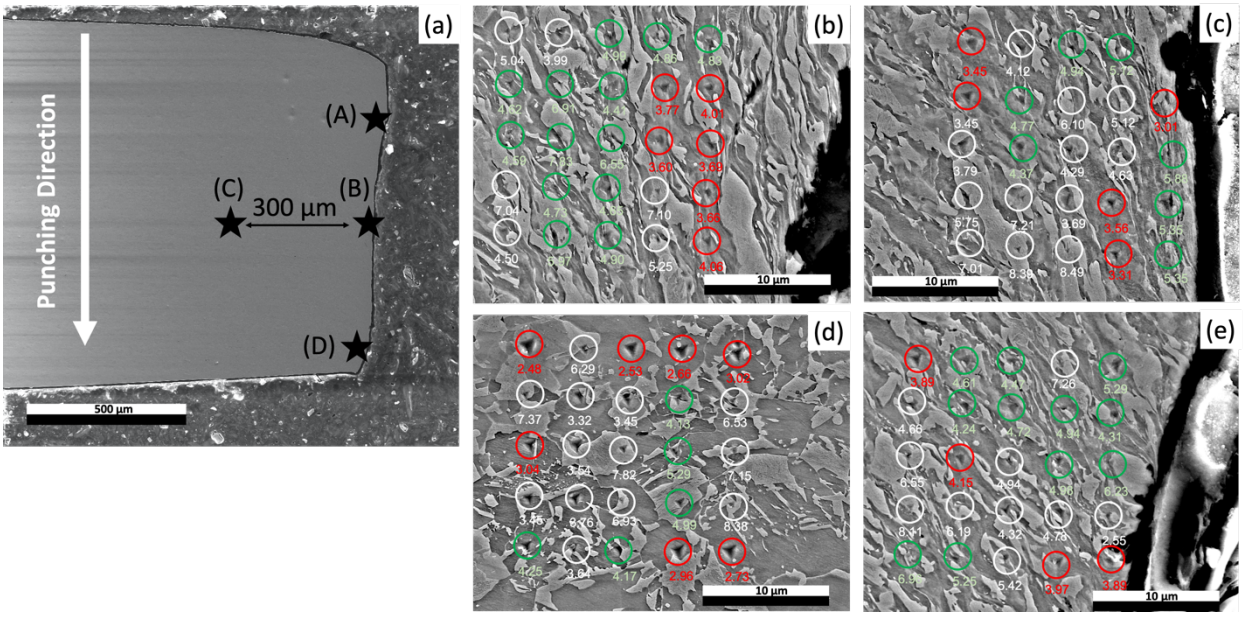

Figure 10 Nanoindentation tests for the initial punched hole sheared edge of the fully annealed DP steels with SC anneals. (**a**) The SEM micrograph schematically illustrating the tested positions. The SEM micrographs as well as nano-indents of (**b**) position A, (**c**) position B, (**d**) position C and (**e**) position D with the high magnification.

The measured nanohardness values of ferrite and major hard constituents (fresh martensite (for GI anneals) and tempered martensite (for SC anneals)) in the tested regions of the selected fully annealed DP steels with both GI and SC anneals are listed in Table 3. These results are also compared with their counterparts in the undeformed conditions, Table 3. Prior to hole punching, the nanohardness values of ferrite and fresh martensite for sample A1, GI are 3.1 GPa and 8.0 GPa, respectively. Regarding the SC annealed DP sample A1, SC, the nanohardness data of ferrite and tempered martensite are 2.6 GPa and 4.1 GPa, respectively. In the wake of hole punching, the deformed ferrite near the initial punched hole sheared edge (i.e., positions (A), (B) and (D)) of GI annealed sample A1, GI can be hardened by the internal plastic strains and the nanohardness can increase from 3.1 GPa to 5.7 GPa (~83% increase) at position (B). In the same way, the nanohardness values of the fresh martensite can increase about 21% ~ 40% in positions (A), (B) and (D), reaching the maximum value of 11.2 GPa. Considering the deformed final microstructures

in positions (A), (B) and (D) of the SC annealed condition A1, SC, the nanohardness results of ferrite can increase to the maximum value of 3.8 GPa (~46% increase) at position (A). The tempered martensite can also be strengthened by a large amount of plastic deformation near the initial punched hole sheared edge, possessing the nanohardness values of 5.0-5.4 GPa (~20%-32% increase). However, in the position (C), 300 μm away from the initial punched hole sheared edges of both GI and SC annealed samples, the effect of work hardening on the nanohardness of ferrite and hard constituents (fresh martensite (for GI anneals) and tempered martensite (for SC anneals)) is not significant. These results indicate that hole punching damage near the initial punched hole sheared edge is very large, especially for the GI annealed DP steels, which will severely influence the HER values in the subsequent hole expanding phase of the test after hole expanding.

Table 3

The nanohardness of the tested positions of the initial punched hole sheared edges for the selected fully annealed DP steels with both GI and SC steels

IDs	Phases	Nanohardness (GPa)				
		Undeformed	Position (A)	Position (B)	Position (C)	Position (D)
A1, GI	Ferrite	3.1±0.5	5.4±0.4	5.7±0.5	3.8±0.4	5.4±0.7
	Fresh Martensite	8.0±0.6	11.2±1.4	9.7±1.9	8.9±0.6	10.9±0.3
A1, SC	Ferrite	2.6±0.4	3.8±0.2	3.4±0.2	2.8±0.2	3.9±0.1
	Tempered Martensite	4.1±0.5	5.4±1.1	5.1±0.5	4.6±0.5	5.0±0.8

4. Discussion

4.1 The influences of coiling temperature and annealing path on final microstructures and tensile properties

Prior to describing the effects of coiling temperatures on microstructural features of fully annealed DP steels, an important concept of stored energy [48,49] needs to be introduced first. Stored energy, associated with the lattice defects, mainly dislocations, results from the cumulative effects of the transformation strains associated with the decomposition of austenite during the coiling of the hot band coils and later by the plastic deformation in cold rolling. From previous studies [42,47], the combination of low coiling temperatures and high cold reductions introduced more dislocations into the ferrite, providing a large driving force for ferrite recrystallization and

austenite formation during intercritical annealing at a short holding time. Also, in this research, the low coiling temperature combined with a constant reduction (~60%) can give rise to a higher amount of intercritically formed austenite and a higher volume percentage of hard components (i.e., fresh martensite, bainite and/or tempered martensite) as can be observed after full CGL simulations. In addition, the effect of annealing path on the final microstructures after full CGL simulations is of significance. The change in annealing path, from standard galvanizing to supercooling process, results in the replacement of fresh martensite with tempered martensite

The effect of a low coiling temperature on tensile strength is ascribed to the stored energy caused by phase transformation. A low coiling temperature (CT=580°C) results in the formation of acicular ferrite or intermediate-temperature ferrite with a high dislocation density or more sub-structures [50]. These dislocation structures provide a high driving force for the transformation of intercritically formed austenite in an intercritical or two phase ($\alpha+\gamma$) region. After fast cooling, a large amount of austenite transforms into fresh martensite, hence leading to a higher UTS with the sacrifice of TE. Additionally, the influences of annealing path on tensile properties are obvious. The change in annealing path, from standard galvanizing to supercooling process, results in the replacement of hard fresh martensite with soft tempered martensite. A large volume fraction of tempered martensite contributes to a good total elongation.

4.2 Crack initiation originated from punching

The hole punching process generates two regions, initial punched hole surface (Figure 5) and initial punched hole sheared edge (Figure 6). Micro-voids and shearing dimples in the fracture zone of the initial punched hole surface are introduced by punching ((Figures 5 (d) (e)). These defects caused by punching act as the crack initiation sites [31,34–38] and later severely influence hole expansion performances during hole expanding. Hence, HER values can be improved significantly when these initial punched defects removed by other hole forming methods (i.e., laser cutting, water jetting, drilling and EDM [13]) or post-punching approaches [24].

In addition, the micro-voids or micro-cracks observed in the regions of initial punched hole sheared-edge (Figures 6 (d), (e), (h)), are in agreement with the two major void nucleation mechanisms [34–36], martensite cracking and the decohesion of ferrite/hard constituent (i.e., bainite, fresh martensite and tempered martensite) interfaces. Also, the observation of the micro-cracks associated with MnS or MnS & ZrO_3 inclusions (Figures 6 (b) and (f)) is in agreement with

Okano's work that the voids nucleated at the ferrite/inclusion (MnS) or ferrite/precipitate (TiN or TiS) interfaces [37].

In the early stage of hole expansion, cracks start to propagate, or voids start to grow by void enlargement, coexisting with continuing void nucleation, as plastic strain increases. With further deformation, cracks continue propagating from the fracture zone towards the burnished and rollover zones. Once the major crack crosses the thickness of the tested sample, the test is, by definition, completed, and at which point the HET is stopped.

4.3. The effect of coiling temperature on stretch-flangeability

The effects of coiling temperature on the final microstructures and mechanical properties of the fully annealed DP steels with both GI and SC anneals are presented in Tables 1 and 2. Decreasing the coiling temperatures from 677°C to 580°C refines the ferrite grains for all steel conditions, which is beneficial to HER, UTS and TE results, Tables 1 and 2. The initial microstructures of the hot band coils with a low coiling temperature of 580°C, prior to cold rolling and intercritical annealing, mainly consist of pearlite and refined acicular ferrite with high dislocation density and more sub-structures, while the structures for the DP steels coiled at 677°C consist of coarse polygonal ferrite with low dislocation density [50]. The difference in the dislocation density of these two types of ferrite leads to the apparent difference in the stored energy for the steels with different coiling temperatures. The pre-annealing condition of a low coiling temperature (580°C) and 60% cold reduction results in high stored energy, providing more driving force for ferrite recrystallization and the austenite nucleation and growth in the limited annealing soaking time. As a result, the effect of this pre-annealing combination is a higher volume percentage of hard constituents (bainite, fresh martensite or tempered martensite) for both GI and SC anneals, Figures 1, 2 and Table 1. From Davies' research [2], tensile strength is dependent on the amount of fresh martensite, ferrite grain sizes and second phase precipitates within the ferrite. Therefore, the UTS increases as the coiling temperature falls, Table 2.

Figure 11 shows the trends of hole expansion performances and average ferrite grain sizes as the coiling temperature decreases from 677°C to 580°C for the fully annealed DP steels with both GI and SC anneals. As mentioned above, lowering coiling temperatures results in finer ferrite grains in the final microstructures. The effects of ferrite grain sizes on stretch-flangeability were investigated by several researchers [28,29]. Fracture toughness is considered a critical factor controlling the sheared-edge ductility of AHSSs [34] and grain refinement is the only effective

approach of improving both tensile strength and fracture toughness. The behavior of void nucleation and growth caused by hole punching at the ferrite/ferrite grain boundaries changes with ferrite grain sizes [29], indicating that fine-grained structures have a higher capability of resisting void propagation and coalescence during hole expanding. So, producing fine-grained or ultra-fine-grained structures is beneficial to stretch-flangeability.

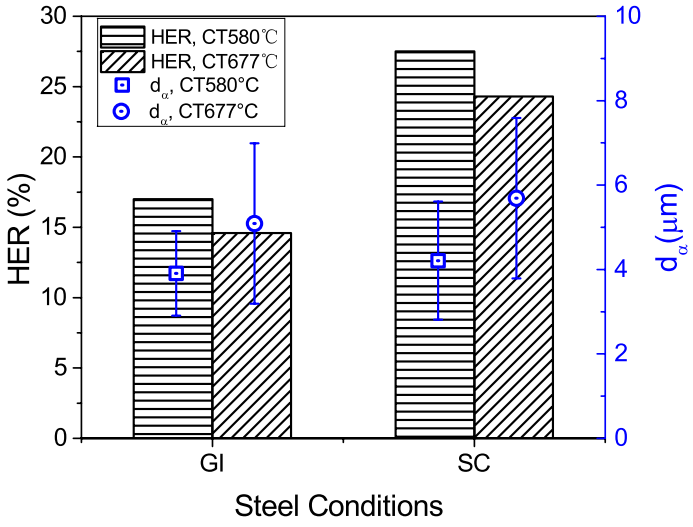

Figure 11 Hole expansion ration (HER, %) vales and average ferrite grain sizes (d_α, μm) for different steel conditions (coiling temperatures and annealing paths). The ferrite grain sizes and standard deviations are shown by the open symbols and error bars.

4.3. The effect of annealing path on stretch-flangeability

There were two CGL simulations studied in this paper, one is GI (standard galvanizing) and the other one is SC (supercooling process), Figure 1. Figure 12 shows the volume fractions of different microstructures for various steel conditions (coiling temperature and CGL simulations). The changes in CGL simulations from GI to SC cause the replacement of hard fresh martensite with soft tempered martensite, Figure 12 and Table 1. Taylor et al [13] emphasized the importance of the nanohardness difference between hard phase martensite and soft phase ferrite on the stretch-flangeability of DP 980 steels. Reducing the nanohardness difference between hard and soft phases can improve the hole expansion behaviors of DP steels [13,42,47]. For instance, the HER value of A1, SC (CT580℃, supercooling process) improves by ~ 62%, compared with the one of A1, GI (CT580℃, standard galvanizing), which is due to the nanohardness difference for undeformed

microstructures of ferrite and martensite from 4.9 GPa (steel condition A1, GI) to 1.5 GPa (A1, SC) for the difference between the undeformed ferrite and tempered martensite.

Another factor causing the difference in the HER values between GI and SC annealed DP steels is the different internal strains introduced by hole punching prior to hole expanding. The KAM and estimated ε_{eq} values (Figure 8) or the nanohardness results of the work hardened microstructures (Figures 9, 10 and Table 3) indicate that the punching introduces different levels of internal strains and hence causes discrete damages for both GI and SC annealed DP steels. Concerning the initial punched hole sheared edge near the burnished and fracture transition zone, punching introduced the ε_{eq} of 2.92 to a GI annealed steel sample (A1, GI), causing ferrite and fresh martensite to be work hardened from 3.1 GPa to 5.4 GPa and from 8.0 GPa to 11.2 GPa, respectively, in this region. For SC annealed condition (A1, SC), punching introduced less internal plastic strain (ε_{eq} = 1.48), making the nanohardness values of ferrite and tempered martensite to be increased from 2.6 GPa to 3.8 GPa and from 4.1 GPa to 5.4 GPa, respectively in this region. So, the less internal plastic strains or damage caused by punching enable SC annealed DP steels to obtain better shear-edge ductility before final fracture.

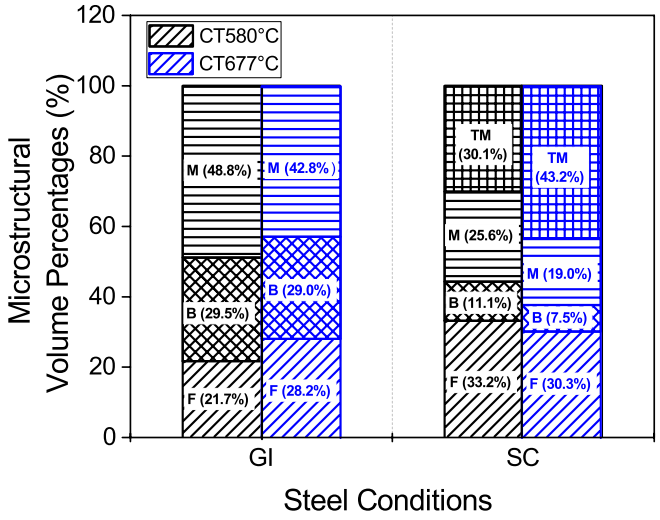

Figure 12 Microstructural volume percentages of different steel conditions (coiling temperatures and annealing paths). Note ferrite is labeled by F, bainite by B, fresh martensite by M and tempered martensite by TM.

5. Conclusions

The purpose of this study was to improve the understanding of stretch-flangeability of ultra-high strength DP steels. The candidate DP steel was designed and processed with different coiling temperatures and CGL simulations. The effects of coiling temperatures and CGL simulations (especially the supercooling process) on the sheared-edge ductility of DP steels were investigated. Also, the crack initiation caused by hole punching, which can severely influence sheared-edge ductility was studied. The following conclusions were obtained**.**

1. A low coiling temperature of 580°C with the standard galvanizing process can obtain a high martensite volume fraction and fine-grained microstructures with a high UTS of 1092.8 MPa and a reasonable TE of 20.8 %.
2. The changes in the CGL simulations from standard galvanizing to the supercooling process resulted in the replacement of fresh martensite with tempered martensite in microstructures. These changes also reduced the nanohardness difference between ferrite and hard phase constituents, hence remarkably improving stretch flangeability.
3. Hole punching process prior to hole expanding had a critical influence on the hole expansion performance of the DP conditions studied. Micro-voids and shearing dimples in the fracture zone of the initial punched hole surface were introduced by hole punching. Additionally, internal plastic strains near the initial punched hole sheared edges were increased due to hole punching. Taken together, these two types of damage appeared to severely influence the sheared-edge ductility and HER.

References

[1] R.G. Davies, The deformation behavior of a vanadium-strengthened dual phase steel, Metall. Trans. A. 9 (1978) 41–52. https://doi.org/10.1007/BF02647169.

[2] R.G. Davies, Influence of martensite composition and content on the properties of dual phase steels, Metall. Trans. A. 9 (1978) 671–679. https://doi.org/10.1007/BF02659924.

[3] R.G. Davies, Early stages of yielding and strain aging of a vanadium-containing dual-phase steel, Metall. Trans. A. 10 (1979) 1549–1555. https://doi.org/10.1007/BF02812021.

[4] R.G. Davies, C.L. Magee, Physical metallurgy of automotive high-strength steels, JOM. 31 (1979) 17–23. https://doi.org/10.1007/BF03354565.

[5] G.R. Speich, V.A. Demarest, R.L. Miller, Formation of austenite during intercritical annealing of dual-phase steels, Metall. Mater. Trans. A. 12 (1981) 1419–1428. https://doi.org/10.1007/BF02643686.

[6] G.R. Speich, Physical metallurgy of dual-phase steels, in: R.A. Kot, B.L. Bramfitt (Eds.), Fundam. Dual-Phase Steels Proc. a Symp., AIME, Chicago, 1981: pp. 3–45.

[7] M.S. Rashid, B.V.N. Rao, Tempering characteristics of a vanadium containing dual phase steel, Metall.

Trans. A. 13 (1982) 1679–1686. https://doi.org/10.1007/BF02647823.
[8] M.S. Rashid, Dual phase steels, Annu. Rev. Mater. Sci. 11 (1981) 245–266. https://doi.org/10.1146/annurev.ms.11.080181.001333.
[9] N.K. Balliger, T. Gladman, Work hardening of dual-phase steels, Met. Sci. 15 (1981) 95–108. https://doi.org/10.1179/030634581790426615.
[10] A.R. Marder, The effect of heat treatment on the properties and structure of molybdenum and vanadium dual-phase steels, Metall. Trans. A. 12 (1981) 1569–1579. https://doi.org/10.1007/BF02643562.
[11] C.I. Garcia, M. Hua, K. Cho, K. Redkin, A.J. DeArdo, Metallurgy and continuous galvanizing line processing of high-strength dual-phase steels microalloyed with niobium and vanadium, Metall. Ital. 104 (2012) 3–8.
[12] M.P. Rao, V.S. Sarma, S. Sankaran, Development of high strength and ductile ultra fine grained dual phase steel with nano sized carbide precipitates in a V–Nb microalloyed steel, Mater. Sci. Eng. A. 568 (2013) 171–175. https://doi.org/10.1016/j.msea.2012.12.084.
[13] M.D. Taylor, K.S. Choi, X. Sun, D.K. Matlock, C.E. Packard, L. Xu, F. Barlat, Correlations between nanoindentation hardness and macroscopic mechanical properties in DP980 steels, Mater. Sci. Eng. A. 597 (2014) 431–439. https://doi.org/10.1016/j.msea.2013.12.084.
[14] Y. Gong, The mechanical properties and microstructures of vanadium bearing high strength dual phase steels processed with continuous galvanizing line simulations, University of Pittsburgh, 2015.
[15] C.C. Tasan, M. Diehl, D. Yan, M. Bechtold, F. Roters, L. Schemmann, C. Zheng, N. Peranio, D. Ponge, M. Koyama, K. Tsuzaki, D. Raabe, An overview of dual-phase steels: advances in microstructure-oriented processing and micromechanically guided design, Annu. Rev. Mater. Res. 45 (2015) 391–431. https://doi.org/10.1146/annurev-matsci-070214-021103.
[16] Y. Gong, Y. Wu, M. Hua, J. Uusitalo, A.J. DeArdo, Influence of processing factors on the sheared-edge formability of vanadium bearing dual-phase steels produced using continuous galvanizing line simulations, J. Mater. Sci. 55 (2020) 5639–5654. https://doi.org/10.1007/s10853-020-04385-0.
[17] N. Fonstein, Advanced High Strength Sheet Steels, 2015. https://doi.org/10.1007/978-3-319-19165-2.
[18] A.K. Sachdev, Effect of retained austenite on the yielding and deformation behavior of a dual phase steel, Acta Metall. 31 (1983) 2037–2042. https://doi.org/10.1016/0001-6160(83)90021-4.
[19] O. Matsumura, Y. Sakuma, H. Takechi, Enhancement intercritical of elongation annealed by retained austenite steel, Trans. ISIJ. 27 (1987) 570–579. https://www.jstage.jst.go.jp/article/isijinternational1966/27/7/27_7_570/_pdf/-char/ja.
[20] Y. Sakuma, O. Matsumura, H. Takechi, Mechanical properties and retained austenite in intercritically heat-treated bainite-transformed steel and their variation with Si and Mn additions, Metall. Trans. A. 22 (1991) 489–498. https://doi.org/10.1007/BF02656816.
[21] H. Huang, O. Matsumura, T. Furukawa, Retained austenite in low carbon, manganese steel after intercritical heat treatment, Mater. Sci. Technol. 10 (1994) 621–626. https://doi.org/10.1179/mst.1994.10.7.621.
[22] J. Chiang, J.D. Boyd, A.K. Pilkey, Effect of microstructure on retained austenite stability and tensile behaviour in an aluminum-alloyed TRIP steel, Mater. Sci. Eng. A. 638 (2015) 132–142. https://doi.org/10.1016/j.msea.2015.03.069.
[23] J. Speer, D.K. Matlock, B.C. De Cooman, J.G. Schroth, Carbon partitioning into austenite after martensite transformation, Acta Mater. 51 (2003) 2611–2622. https://doi.org/10.1016/S1359-6454(03)00059-4.
[24] J.I. Yoon, J. Jung, H.H. Lee, G.-S. Kim, H.S. Kim, Factors governing hole expansion ratio of steel sheets with smooth sheared edge, Met. Mater. Int. 22 (2016) 1009–1014. https://doi.org/10.1007/s12540-016-6346-5.
[25] X. Fang, Z. Fan, B. Ralph, P. Evans, R. Underhill, The relationships between tensile properties and hole expansion property of C-Mn steels, J. Mater. Sci. 38 (2003) 3877–3882. https://doi.org/10.1023/A:1025913123832.
[26] J.H. Kim, Y.J. Kwon, T. Lee, K.-A. Lee, H.S. Kim, C.S. Lee, Prediction of hole expansion ratio for various steel sheets based on uniaxial tensile properties, Met. Mater. Int. 24 (2018) 187–194. https://doi.org/10.1007/s12540-017-7288-2.
[27] A. Kamp, S. Celotto, D.N. Hanlon, Effects of tempering on the mechanical properties of high strength dual-phase steels, Mater. Sci. Eng. A. 538 (2012) 35–41. https://doi.org/10.1016/j.msea.2012.01.008.
[28] J.I. Yoon, H.H. Lee, J. Jung, H.S. Kim, Effect of grain size on stretch-flangeability of twinning-induced plasticity steels, Mater. Sci. Eng. A. 735 (2018) 295–301. https://doi.org/10.1016/j.msea.2018.08.052.
[29] H. Gwon, J.H. Kim, J.-K. Kim, D.-W. Suh, S.-J. Kim, Role of grain size on deformation microstructures and stretch-flangeability of TWIP steel, Mater. Sci. Eng. A. 773 (2020) 138861.

https://doi.org/10.1016/j.msea.2019.138861.
[30] O.R. Terrazas, K.O. Findley, C.J. Van Tyne, Influence of martensite morphology on sheared-edge formability of dual-phase steels, ISIJ Int. 57 (2017) 937–944. https://doi.org/10.2355/isijinternational.ISIJINT-2016-602.
[31] K. Hasegawa, K. Kawamura, T. Urabe, Y. Hosoya, Effects of microstructure on stretch-flange-formability of 980 MPa grade cold-rolled ultra high strength steel sheets, ISIJ Int. 44 (2004) 603–609. https://doi.org/10.2355/isijinternational.44.603.
[32] K. Hasegawa, S. Kaneko, K. Seto, Cold-rolled and galvannealed (GA) high strength steel sheets for automotive cabin structure, JFE Tech. Rep. 18 (2013) 80–88.
[33] Y. Gong, M. Hua, J. Uusitalo, A.J. Deardo, Processing factors that influence the microstructure and properties of high-strength dual- phase steels produced using CGL simulations, in: AISTech 2016 Proc., 2016: pp. 2779–2790.
[34] J.I. Yoon, J. Jung, J.G. Kim, S.S. Sohn, S. Lee, H.S. Kim, Key factors of stretch-flangeability of sheet materials, J. Mater. Sci. 52 (2017) 7808–7823. https://doi.org/10.1007/s10853-017-1012-y.
[35] B.S. Levy, M. Gibbs, C.J. Van Tyne, Failure during sheared edge stretching of dual-phase steels, Metall. Mater. Trans. A. 44 (2013) 3635–3648. https://doi.org/10.1007/s11661-013-1718-7.
[36] N. Pathak, C. Butcher, M. Worswick, E. Bellhouse, J. Gao, Damage evolution in complex-phase and dual-phase steels during edge stretching, Materials (Basel). 10 (2017) 346. https://doi.org/10.3390/ma10040346.
[37] T. Okano, C. Inoue, S. Suzuki, K. Yamazaki, S. Toyoda, Reduction of Cracks During Punching Process by Cementite in High Tensile Strength Steel Sheets, Metall. Mater. Trans. A Phys. Metall. Mater. Sci. 50 (2019) 884–893. https://doi.org/10.1007/s11661-018-5043-z.
[38] T. Sirinakorn, V. Uthaisangsuk, S. Srimanosaowapark, Effects of the tempering temperature on mechanical properties of dual phase steels, J. Met. Mater. Miner. 24 (2014) 13–20. https://doi.org/10.14456/jmmm.2014.3.
[39] K. Sugimoto, A. Nagasaka, M. Kobayashi, S. Hashimoto, Effects of retained austenite parameters on warm stretchflangeability in TRIP-aided dual-phase sheet steels., ISIJ Int. 39 (1999) 56–63. https://doi.org/10.2355/isijinternational.39.56.
[40] D.Z. Yang, E.L. Brown, D.K. Matlock, G. Krauss, Ferrite recrystallization and austenite formation in cold-rolled intercritically annealed steel, Metall. Trans. A. 16 (1985) 1385–1392. https://doi.org/10.1007/BF02658671.
[41] J. Huang, W.J. Poole, M. Militzer, Austenite formation during intercritical annealing, Metall. Mater. Trans. A. 35 (2004) 3363–3375. https://doi.org/10.1007/s11661-004-0173-x.
[42] Y. Wu, A.J. Deardo, Processing , microstructures and properties of ultra- high strength , low varbon and V-bearing dual-phase steels produced on continuous galvanizing lines, in: Mater. Sci. Technol. 2018, MS T 2018, 2018: pp. 454–463. https://doi.org/10.7449/2018/MST_2018_454_463.
[43] P.A. Soloski, N.J. Thimons, A.A. Marks, J. Hartle, Q. Trest, A. Johnston, W. Perisse, A.J. DeArdo, Sheared-edge ductility / hole-expansion ratio testing of advanced high-strength steels, in: Mater. Sci. Technol. 2015, Columbus, 2015: pp. 917–926.
[44] S.I. Wright, M.M. Nowell, D.P. Field, A review of strain analysis using electron backscatter diffraction, Microsc. Microanal. 17 (2011) 316–329. https://doi.org/10.1017/S1431927611000055.
[45] M. Calcagnotto, D. Ponge, E. Demir, D. Raabe, Orientation gradients and geometrically necessary dislocations in ultrafine grained dual-phase steels studied by 2D and 3D EBSD, Mater. Sci. Eng. A. 527 (2010) 2738–2746. https://doi.org/10.1016/j.msea.2010.01.004.
[46] N. Nakada, K. Ikeda, H. Shuto, T. Yokoi, T. Tsuchiyama, S. Hata, H. Nakashima, S. Takaki, Quantification of large deformation with punching in dual phase steel and change of its microstructure –Part II: Local strain mapping of dual phase eteel by a combination technique of electron backscatter diffraction and digital image correlation methods, ISIJ Int. 56 (2016) 2077–2083. https://doi.org/10.2355/isijinternational.ISIJINT-2016-310.
[47] Y. Gong, J. Uusitalo, M. Hua, Y. Wu, A.J. DeArdo, Effects of pre-annealing conditions on the microstructure and properties of vanadium-bearing dual-phase steels produced using continuous galvanizing line simulations, J. Mater. Sci. 54 (2019) 7211–7230. https://doi.org/10.1007/s10853-019-03338-6.
[48] S.H. Choi, Y.S. Jin, Evaluation of stored energy in cold-rolled steels from EBSD data, Mater. Sci. Eng. A. 371 (2004) 149–159. https://doi.org/10.1016/j.msea.2003.11.034.
[49] C. Fang, C.I. Garcia, S.-H. Choi, A.J. DeArdo, A Study of the batch annealing of cold-rolled HSLA steels containing niobium or titanium, Metall. Mater. Trans. A. 46 (2015) 3635–3645. https://doi.org/10.1007/s11661-015-2949-6.

[50] G. Krauss, S.W. Thompson, Ferritic microstructures in continuously cooled low- and ultralow-carbon steels., ISIJ Int. 35 (1995) 937–945. https://doi.org/10.2355/isijinternational.35.937.
[51] B.S. Levy, C.J. Van Tyne, Review of the shearing process for sheet steels and its effect on sheared-edge stretching, J. Mater. Eng. Perform. 21 (2012) 1205–1213. https://doi.org/10.1007/s11665-011-9997-x.